Editors' Suggestion

Forced symmetry breaking as a mechanism for rogue bursts in a dissipative nonlinear dynamical lattice

P. Subramanian [1,2] E. Knobloch,[3] and P. G. Kevrekidis [4]

[1]*Department of Mathematics, University of Auckland, 38 Princes Street, Auckland 1010, New Zealand*

[2]*Mathematical Institute, University of Oxford, Oxford OX2 6GG, United Kingdom*

[3]*Department of Physics, University of California at Berkeley, Berkeley, California 94720, USA*

[4]*Department of Mathematics and Statistics, University of Massachusetts, Amherst, Massachusetts 01003-4515, USA*

(Received 18 March 2022; accepted 31 May 2022; published 27 July 2022)

We propose an alternative to the standard mechanisms for the formation of rogue waves in a nonconservative, nonlinear lattice dynamical system. We consider an ordinary differential equation (ODE) system that features regular periodic bursting arising from forced symmetry breaking. We then connect such potentially exploding units via a diffusive lattice coupling and investigate the resulting spatiotemporal dynamics for different types of initial conditions (localized or extended). We find that in both cases, particular oscillators undergo extremely fast and large amplitude excursions, resembling a rogue wave burst. Furthermore, the probability distribution of different amplitudes exhibits bimodality, with peaks at both vanishing and very large amplitude. While this phenomenology arises over a range of coupling strengths, for large values thereof the system eventually synchronizes and the above phenomenology is suppressed. We use both distributed (such as a synchronization order parameter) and individual oscillator diagnostics to monitor the dynamics and identify potential precursors to large amplitude excursions. We also examine similar behavior with amplitude-dependent diffusive coupling.

DOI: 10.1103/PhysRevE.106.014212

I. INTRODUCTION

The formation of rogue waves or spatiotemporal bursts has been investigated by a number of authors [1,2] and different mechanisms leading to such waves have been identified. Relevant approaches include completely linear mechanisms (e.g., a superposition of multiple linear waves) or fully nonlinear mechanisms (e.g., modulational instability of a uniform wave train) [3,4]. Some of the original observations stem from the study of North Sea waves [5–8], but more recent work has extended similar considerations not only to other areas of the oceans but also to numerous other scientific areas where controlled laboratory experiments are available. These include studies of sloshing of water waves in large tanks [9–12] and the realm of nonlinear optics [13–16], with some work spanning both areas (see, e.g., [12]). Attempts to establish rogue wave emergence as a property of a broad class of physics-based models have been reported in ultracold atomic Bose-Einstein condensates [17], in space plasmas [18–21] and elsewhere [22].

Arguably, a large portion of the relevant efforts to generate rogue waves has revolved around models of dissipationless dispersive wave propagation, with the nonlinear Schrödinger (NLS) equation [23,24] and its variants providing the central model in this direction. Given that the NLS equation describes the slow evolution of a packet of small amplitude dispersive waves, nonlinear effects are key to the formation of large amplitude rogue burst events. In this context, specific nonlinear solutions, such as the Peregrine soliton [25], the periodic in time Kuznetsov-Ma soliton [26,27], and the periodic in space Akhmediev breather [28], have been central to numerous investigations. However, as is well known, such exactly integrable settings and the analytical solutions available via the inverse scattering transform (and related approaches) are rather rare, especially so in higher-dimensional settings.

Many of the above ideas on identifying rogue events in integrable systems have also been extended to lattice models such as the integrable Ablowitz-Ladik system [29], the nonintegrable discrete NLS equation [30], and the Salerno system which homotopically interpolates between the two. Rogue events in such lattice models are a consequence of nonlinear effects arising from modulational instability. However, conservation laws (if present) prohibit arbitrarily large responses and limit the norm at any lattice node to the initial norm. Such constraints do not play a role in the dynamics of dissipative lattice systems such as the model considered in this work, allowing rogue wave behavior arising from fundamentally distinct physical mechanisms. It is thus of considerable interest to explore such alternative mechanisms given their potentially broader applicability and straightforward extension to higher dimensions. Indeed, the recent work of [31] captures the relevant motivation well in the statement: "from the general point of view, the identification of the necessary ingredients for the emergence of rogue waves and extreme events in dissipative systems remains a challenging open problem."

Here we focus on the fundamentally spatiotemporal nature of the localization of rogue waves and their defining property of "appearing out of nowhere and disappearing without a trace" [32] but employ an approach that does not rely on the Hamiltonian nature of the problem or on its integrability

properties. In dissipative systems sustained rogue wave formation requires the presence of forcing. To capture the essence of rogue waves this forcing must be uniform in space. In this work we leverage the properties of a model problem studying the interaction properties of standing waves in domains of moderate aspect ratio, following [33,34]. This dissipative system satisfies the above requirement where waves arise via a Hopf bifurcation from a trivial state. With Neumann boundary conditions these waves may be of even or odd parity under spatial reflection, and in moderately large domains such waves are nearly degenerate with an approximate interchange symmetry between them, resulting in strong interaction. The state of the system is described by a pair of coupled equations for the two wave amplitudes given by the normal form for a Hopf bifurcation with broken D_4 symmetry. This symmetry is a consequence of spatial reflection together with the approximate interchange symmetry between the two modes; the symmetry is broken because the interchange symmetry is not exact, and sample integration of the resulting equations reveals intermittent bursts with amplitudes as large as 10^9 [35]. We refer to these solutions as bursts to emphasize they are localized in time but not in space. The resulting system explains successfully the presence of bursts in experiments including those on binary fluid convection in domains of moderate aspect ratio [33,36].

Within the above formulation the spatial degrees of freedom are inevitably slaved to the temporal dynamics of the mode amplitudes. In order to activate spatial degrees of freedom over yet larger length scales, we consider here a ring of identical, diffusively coupled oscillators of the above type, each of which can generate a large spatially coherent burst (or a sequence of such bursts), depending on parameters. We use the ring geometry in order to generate a spatially periodic system, i.e., to mimic a very large aspect ratio system where local regions remain spatially coherent. The resulting model has the advantage that the dynamics of each oscillator is well understood. In particular, it is understood that the broken D_4 symmetry permits the trajectory of each individual oscillator to escape to infinity in finite time and to return from infinity, also in finite time, even when the even and odd standing waves both bifurcate supercritically. On a ring of such oscillators the resulting excitation may be localized at one site, or a small group of adjacent sites, resulting in the generation of a temporally *and* spatially localized extreme event, i.e., a rogue wave.

We demonstrate here, via direct numerical simulations, that for weak coupling the above system exhibits rogue events apparently occurring at "random" times and at "random" locations. Importantly, this is the case even when the parameters characterizing the individual oscillators are chosen to generate periodic oscillations only. We offer different diagnostics ranging from the event amplitude distribution function to studying the precursors to the local emergence of large amplitude events, in an effort to obtain diverse perspectives towards a qualitative understanding of the relevant phenomenology. This is followed by an investigation of progressively larger coupling, eventually leading to the synchronization of the entire lattice, as well as couplings that vary over space or time, depending on the site amplitude. For this purpose we leverage various synchronization diagnostics such as the Kuramoto order parameter [37]. Our hope is that this initial study will provide motivation for further exploration of alternative mechanisms producing extreme events, and potentially enable their identification in other nonlinear lattice systems in one or more dimensions.

The presentation of our results is structured as follows. In Sec. II, we describe the basic formulation of the model, its parameters, and initial conditions at the ordinary differential equation (ODE) level, first for a single node and subsequently for the diffusively coupled network. In the latter setting, we present the main phenomenology of the system, the diagnostic tools of interest, and the resulting findings for different values of the coupling parameter, as well as for amplitude-dependent coupling. Finally, in Sec. III, we summarize our findings and point to some directions for future study. The Appendix presents some further details on the dynamics of the ODEs on a single node of the lattice.

II. MODEL

A. An oscillator with approximate D_4 symmetry

The dynamics near onset in a system exhibiting a Hopf bifurcation with broken D_4 symmetry, i.e., on a domain of moderate length, is described by the truncated equations

$$\dot{z}_\pm = [\lambda \pm \triangle\lambda + i(\omega \pm \triangle\omega)]z_\pm + A(|z_+|^2 + |z_-|^2)z_\pm + B|z_\pm|^2 z_\pm + C\bar{z}_\pm z_\mp^2. \quad (1)$$

Here $z_\pm$ are the complex amplitudes of the even and odd standing wave modes, the parameters $\triangle\lambda$ and $\triangle\omega$ measure the differences in their linear growth rates and onset frequencies, respectively, while A, B, and C are complex coefficients. When $\triangle\lambda = \triangle\omega = 0$ the two modes follow the same evolution equations and the interchange symmetry between them is exact. Thus, the parameters $\triangle\lambda$ and $\triangle\omega$ represent terms that reflect the fact that the two competing standing modes are not in general identical. Equations (1) assume that in a moderately large domain this effect can be captured at linear order, i.e., via the inclusion of small differences in the growth rates and frequencies of the two competing modes [33].

New variables $\mathcal{A}$, θ, and ϕ defined in [33,34] allow us to completely characterize the solutions of the system with exact D_4 symmetry ($\triangle\lambda = \triangle\omega = 0$) in terms of three qualitatively different periodic solutions, hereafter u, v, and w. Writing

$$z_\pm = \mathcal{A}^{\frac{1}{2}} \sin\left(\theta + \frac{\pi}{4} \pm \frac{\pi}{4}\right) \exp\left(i\frac{(\pm\phi + \psi)}{2}\right), \quad (2)$$

the u solutions correspond to $\cos\theta = 0$ and $\cos 2\phi = 1$, the v solutions correspond to $\cos\theta = 0$ and $\cos 2\phi = -1$, and the w solutions correspond to $\sin\theta = 0$. A fourth solution, a quasiperiodic state referred to as qp, is present in a restricted parameter range. When $\triangle\lambda = \triangle\omega = 0$ these states bifurcate simultaneously from the trivial state at $\lambda = 0$, and the u, v, and w states then represent invariant subspaces of the system. This is no longer the case when the interchange symmetry is broken, i.e., $\triangle\lambda \neq 0$, $\triangle\omega \neq 0$. In this case the w states split into two (the even and odd standing oscillations) and the other states are generated only in secondary bifurcations [34]. We mention that in contrast to the w states, the states u and v represent traveling states [33].

When $\triangle\lambda \neq 0$, $\triangle\omega \neq 0$ there may be parameter regimes in Eqs. (1) with no stable small amplitude oscillations near onset, implying that nontrivial dynamics must take place. In particular, it was found that the solutions in this regime can be attracted to an invariant subspace (the u/v subspace) that extends to *infinite* amplitude. Solutions following this subspace reach very high amplitudes, and sample integration of the equations revealed intermittent bursts with amplitudes as large as 10^9 [35]. A detailed study using a rescaled time shows that solutions lying in this invariant subspace are attracted to a saddle point at infinity that is, in turn, connected to a second saddle point at infinity whose stable manifold returns the trajectory back to small amplitude. In terms of the original time the excursion to infinity and back takes a finite time [33,34]. This behavior can be established using the variable $\rho = \mathcal{A}^{-1}$: as $\mathcal{A} \to \infty$, i.e., as $\rho \to 0$, the terms with $\triangle\lambda$ and $\triangle\omega$ drop out, and the D_4 symmetry becomes exact, allowing a complete description of the dynamics near $\rho = 0$.

In the following we consider a parameter combination for which each element in a diffusively coupled ring of such elements is described by Eqs. (1) but only displays regular finite amplitude periodic spiking as in Fig. 3(a) of [33]. As a result, the rogue waves we observe are a consequence of the spatial coupling of the elements and *not* of their individual behavior at the same parameter values. The corresponding parameter values are

$$\lambda = 0.1,\ \triangle\lambda = 0.03,\ \omega = 1,\ \triangle\omega = 0.02,$$
$$A = 1 - 1.5i,\ B = -2.8 + 5i,\ C = 1 + i, \tag{3}$$

and we focus on the generation of extreme events in the resulting *lattice system*.

B. Diffusively coupled ring of N nodes

Our system consists of N identical oscillators on a ring where each of the N nodes is modeled by the dynamics described in Eqs. (1). The oscillators are coupled via nearest-neighbor coupling with diffusion coefficient K,

$$\dot{z}_{\pm,i} = [\lambda \pm \triangle\lambda + i(\omega + \triangle\omega)]z_{\pm,i} + A(|z_{+,i}|^2 + |z_{-,i}|^2)z_{\pm,i} + B|z_{\pm,i}|^2 z_{\pm,i} + C\bar{z}_{\pm,i}z_{\mp,i}^2 + K\Delta_2 z_{\pm,i}. \tag{4}$$

Here, Δ_2 stands for the discrete Laplacian and $i = 1, \ldots, N$.

The model allows us to explore the interplay between regular periodic spiking (at each node, in the absence of any diffusion) and the effects of amplitude redistribution via diffusive coupling. In the limit of $K = 0$, i.e., with no coupling, we expect to recover regular periodic spiking at each node, albeit with a phase that varies randomly from node to node. In the opposite, diffusion-dominated limit with $K \gg 1$, we expect that all nodes display synchronized regular periodic spiking. Hence, as we increase K, we expect to see progressive synchronization as revealed, for example, by the Kuramoto order parameter (see, e.g., [37]). The transition between these two regimes and the associated dynamical phenomenologies that it enables are the central topic of interest in the present work. Our principal aim is to determine whether in some intermediate regime the spiking of a single node, alongside the nearest-neighbor coupling, is able to give rise to a rogue event, offering in this way a viable alternative to the more customary Hamiltonian mechanisms discussed in the Introduction.

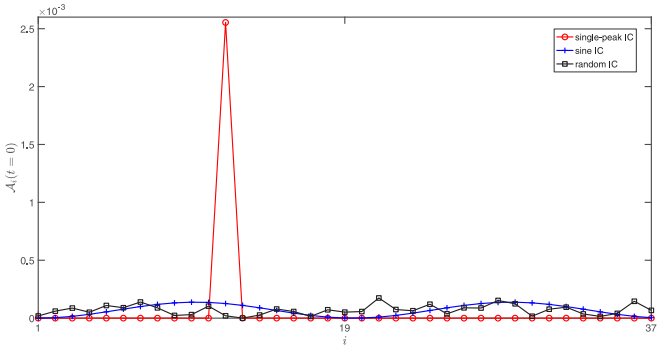

FIG. 1. Three types of initial conditions showing the distribution of initial amplitudes $\mathcal{A}_i(t = 0)$ in a system of $N = 37$ coupled oscillators. The red line with circle markers shows a single peak initial condition, the blue line with crosses shows a sine wave initial condition, and the black line with square markers shows a uniformly distributed random initial condition. In all three cases the Riemann sums pertaining to the three curves are equal.

We choose the number of oscillators in the ring, N, in the range where we can define a distributed initial condition (such as a sine wave function) with sufficient resolution over a wavelength. All results in the rest of this paper are for a system of $N = 37$ oscillators on a ring. Time simulations evolve the system over the time interval $0 < t \leqslant 5000$ and were performed using MATLAB's ode23s subroutine with both relative and absolute tolerance of 1×10^{-5}.

In order to explore the consequence of both localized and extended initial conditions as well as gradients in the initial condition, we choose three types of initial conditions for $z_{\pm}$: a single spike initial condition where $z_{\pm,i}$ is only nonzero at one chosen oscillator, $i = 12$, a smoothly distributed initial condition (more specifically a sine wave such that $z_{\pm}$ reaches maximum at $i = 10, 29$ and minimum at $i = 0, 19$), and a uniformly distributed random initial condition in (0,1). The amplitude $\mathcal{A}_i$ at the ith node at any instant is related to $z_{\pm,i}$ by

$$\mathcal{A}_i = |z_{+,i}|^2 + |z_{-,i}|^2\,, \tag{5}$$

and our initial conditions are such that the sum of $\mathcal{A}_i$ at $t = 0$ over all nodes in the ring is the same. Figure 1 shows a comparison of the three types of initial conditions when $\sum_i \mathcal{A}_i(0) = 2.55 \times 10^{-3}$ in each case.

Figure 2 shows a space-time waterfall plot of the logarithm of the amplitude at each node, $\log_{10}\mathcal{A}_i$, for the case with coupling constant $K = 2.1544 \times 10^{-6}$ and starting from the sine initial condition. During this evolution, the range of variation in $\mathcal{A}_i$ spans eight orders of magnitude, reaching a maximum amplitude excursion of $\mathcal{A}_{19} = 2.28 \times 10^8$ at $t = 2827.5$. The right panel zooms in close to the maximum rogue event to show the sharp and localized excursion in amplitude in more detail, thereby demonstrating that the lattice system is indeed capable of supporting rogue events. In particular we see that, despite the initial sinusoidal variation of amplitude, this sinusoidal pattern is gradually disrupted, and we observe the

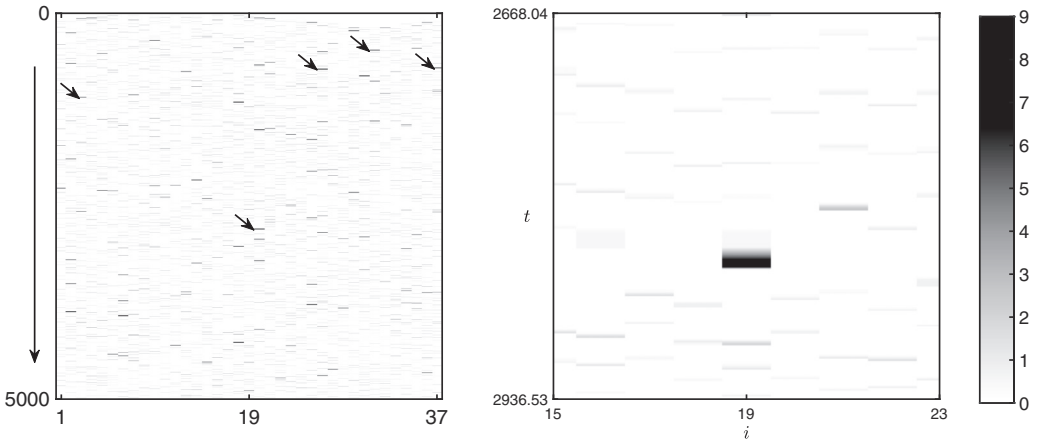

FIG. 2. Left: Space-time plot showing the evolution of $\log_{10}(\mathcal{A}_i)$ starting from a sine initial condition in a system of $N = 37$ coupled oscillators, $1 \leqslant i \leqslant 37$, with $K = 2.1544 \times 10^{-6}$. The diagonal arrows locate the five largest amplitude excursions in this space-time evolution. Right: Zoom of the space-time plot to provide a close-up view of the largest amplitude event in the left panel.

emergence of multiple isolated large amplitude events, shown as black or dark gray events in Fig. 2. The top five amplitude events are highlighted with diagonal arrows to reinforce the unpredictability of their occurrence.

The largest rogue event is shown in finer detail in the zoom in the right panel of Fig. 2. The panels show that at this value of K even immediate neighbors fail to synchronize with the rogue event nearby, as evidenced by the sharp spatial localization of the amplitude. Figure 3 (top panel) confirms this impression in showing the time variation of the amplitude of the oscillator undergoing the maximal amplitude excursion, here $i = 19$ (in black), and two of its immediate neighbors, $i = 18$ (in red) and $i = 20$ (in blue). We observe that even immediate neighbors do not reflect the extremely large amplitude excursion occurring at oscillator $i = 19$.

In contrast, at the larger value $K = 1 \times 10^{-4}$ the neighbors do partially synchronize with the large amplitude event (Fig. 4, left panel) and all evolve to absolute values that are comparable to the maximum amplitude. This is also reflected in Fig. 3 (bottom panel), where the maximum amplitude occurs at $i = 30$ (again in black) but this time this event is also reflected in the amplitude evolution of the two immediate neighbors, $i = 29$ (red) and $i = 31$ (blue). The right panel of Fig. 4 shows that at the yet higher value $K = 2.2 \times 10^{-3}$, all the oscillators synchronize, leading to spatial coherence among all of them.

The large amplitude excursions observed in the left panel of Fig. 2 develop and occur over a very short interval of time and do so irregularly in both space and time, hence their resemblance to a rogue event. In order to understand how frequent such excursions are, we compute the probability density function $p_{\mathcal{A}_{\text{thresh}}}$, which is calculated as the ratio of the number of instances when the amplitude falls between two thresholds, i.e., $\mathcal{A}_{\text{thresh}-1} < \mathcal{A} < \mathcal{A}_{\text{thresh}}$, to the total number of observations over the entire space-time run shown in Fig. 2, left panel. In Fig. 5 we plot the logarithm of the probability density function $p_{\mathcal{A}_{\text{thresh}}}$ using 80 bins spanning the range of amplitudes over the entire space-time run. From the figure we see that the occurrence of very high amplitude events is substantially higher than what would be expected if the distribution of events followed an exponential distribution. The emergent bimodality of the amplitude probability distribution with a second peak corresponding to extremely

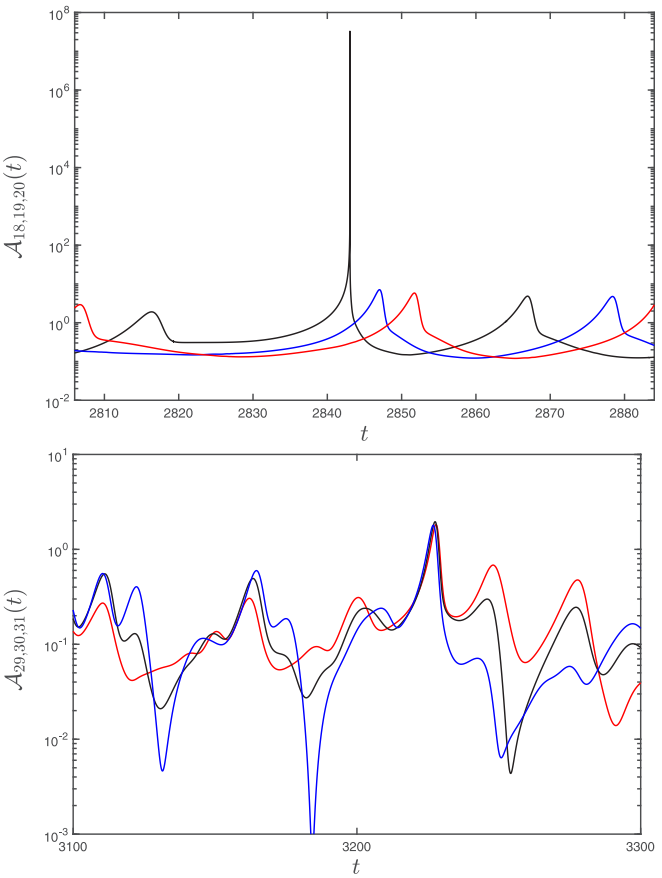

FIG. 3. Top: Evolution of large amplitude event at $i = 19$ (shown as black line) as seen in the right panel of Fig. 2 along with the amplitude evolution of its immediate neighbors at $i = 18$ (red line) and $i = 20$ (blue line). Bottom: Evolution of large amplitude event at $i = 30$ (shown as black line) as seen in the left panel of Fig. 4 along with the amplitude evolution of its immediate neighbors at $i = 29$ (red line) and $i = 31$ (blue line).

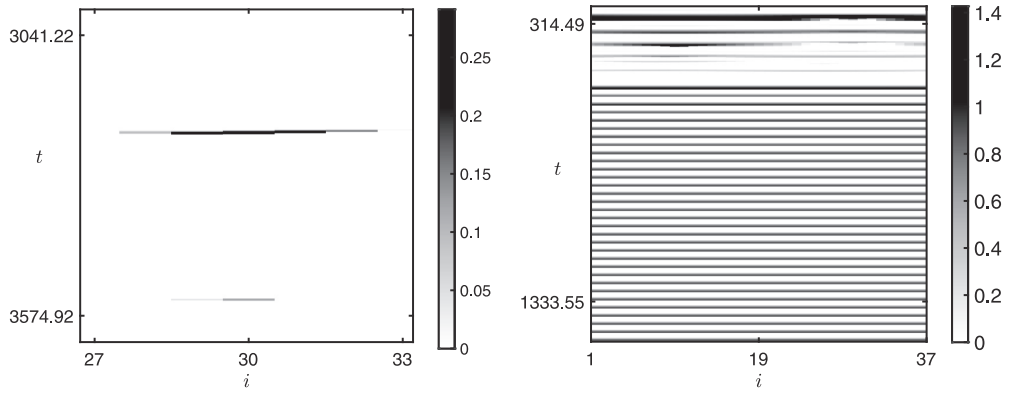

FIG. 4. Space-time plot showing the evolution of $\log_{10}(\mathcal{A}_i)$ starting from a sine initial condition in a system of $N = 37$ coupled oscillators with $K = 1 \times 10^{-4}$ (left panel) with maximum amplitude occurring at $i = 30$, and $K = 2.2 \times 10^{-3}$ (right panel) with maximum amplitude occurring at $i = 10$. The left panel shows that the large amplitude feature is not localized at a single oscillator and that neighboring oscillators respond coherently. In the right panel, all oscillators are synchronized and so oscillate in spatial coherence.

large amplitude events is representative of other, albeit similar, values of the coupling coefficient K as well. It also persists in longer runs with the maximum peak amplitude reached gradually increasing as the run length increases.

We conclude that a diffusively coupled network formed of elements evolving according to Eqs. (1) is capable of generating unpredictable, large amplitude excursions over a short time scale, whose occurrence is more probable than predicted via an exponential distribution of amplitudes. This system is therefore able to produce rogue events. We next look at the effect of varying the coupling coefficient K and describe the resulting changes to the space-time evolution in each case.

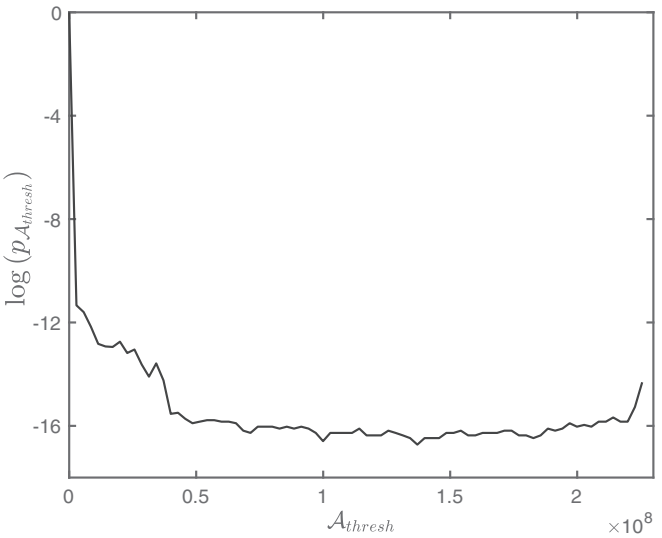

FIG. 5. Logarithm of the probability density function $p_{\mathcal{A}_{\text{thresh}}}$ for different amplitude thresholds $\mathcal{A}_{\text{thresh}}$ from the time evolution shown in Fig. 2. We observe an increase in the probability of extremely large amplitudes, indicating that the occurrence of extreme events is more probable than what is expected from an exponential distribution of amplitudes.

C. Effect of varying K

Having observed the model phenomenology for the special case of weak diffusive coupling ($K = 2.1544 \times 10^{-6}$), we now turn to simulations over a range of diffusion coefficients, $10^{-10} \leqslant K \leqslant 1$, to appreciate the growing role of the coupling. The evolution resulting from the single peak initial condition is shown in Fig. 6 as red lines with circles; that from the sine wave initial condition is shown as blue lines with crosses; and, lastly, the one from the random initial condition is shown in black with square markers.

The top panel in the figure shows the maximum amplitude rogue wave observed over the evolution time, denoted $\mathcal{A}_{\text{max}}$, as a function of K, on a logarithmic scale. This maximum occurs at time $t = t_{\text{max}}$ at the $i = N_{\text{max}}$ node shown in the middle and bottom panels. We see that the maximal excitation remains large until $K \approx 1 \times 10^{-5}$ after which the maximum amplitude abruptly decreases. Beyond this threshold, the diffusion coefficient is large enough to synchronize the nodes. For larger values of K, $\mathcal{A}_{\text{max}}$ increases again, albeit very slowly. For large enough values of K, we recover the regular periodic spiking behavior of a single oscillator for both the sine wave (blue line with crosses) and the random initial condition (black line with square markers). For the single peak initial condition (red line with circles) and large K values, the diffusive coupling overcomes driving at each oscillator and the amplitude decays during subsequent evolution from the initial amplitude $\mathcal{A}_i(t = 0)$ at every node i. For these evolutions, $\mathcal{A}_{\text{max}}$ corresponds to the initial amplitude, which is $\mathcal{O}(10^{-4})$.

The middle panel shows the time $t = t_{\text{max}}$ taken to reach the maximal excitation. For very low values of K we observe that large amplitude excitations occur later in the case of a sine wave initial condition (compared to the other two initial conditions). At large values of K (in the synchronized range), the largest amplitude excursions occur during transient evolution before all the oscillators reproduce the regular periodic oscillations expected from a single uncoupled oscillator. In the case of a single peak initial condition (red line with circles), $t_{\text{max}} = 0$ once we reach the range of K values where the initial

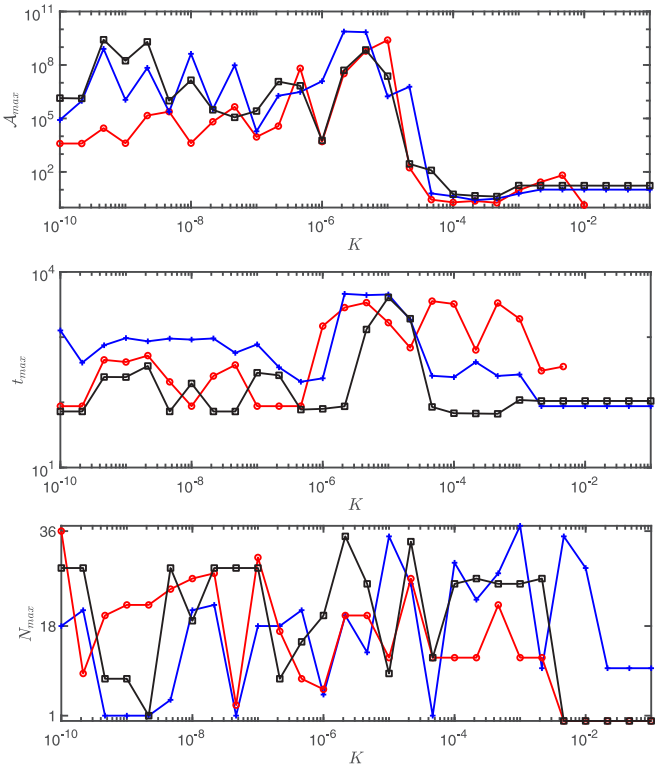

FIG. 6. Red lines with circles show the results for the single peak initial condition, blue lines with crosses show the results for the sine wave initial condition, while black lines with square markers show results for the random initial condition. The top panel shows the variation in the maximum amplitude $\mathcal{A}_{\max}$ (on logarithmic scale) as a function of the diffusion coefficient K. The middle panel shows the time $t_{\max}$ taken to reach the maximal excitation, also on logarithmic scale, while the bottom panel shows the variation of the location $i = N_{\max}$ of that maximal event among the individual oscillators.

amplitude decays with subsequent evolution, and this scenario is therefore not represented in the log-log plot of $t_{\max}$ vs K.

The bottom panel shows the location $i = N_{\max}$ of the maximal excitation as a function of K. We observe that, irrespective of the initial condition, the location of the maximum amplitude is unpredictable; when K is large the synchronized nature of the dynamics also leads to large scatter in $N_{\max}$ but this scatter is no longer meaningful.

In order to measure the effect of varying K on synchronization between the nodes in this network, we compute the Kuramoto order parameter (discussed in detail in, e.g., [37]) for the space-time evolution at each value of the coupling parameter K. We measure the instantaneous degree of phase coherence using the quantity $r(t)$ defined by

$$r(t) = \left| \frac{1}{N} \sum_{j=1}^{N} e^{i\theta_j} \right|, \tag{6}$$

where $\theta_j = \tan^{-1}(\mathrm{Im}(z_+)/\mathrm{Re}(z_+))$, and take the asymptotic value of r, $r_a \equiv \lim_{t\to\infty} r(t)$, as representing the level of synchronization for the chosen level of diffusive coupling [$r(t)$ calculated with z_- shows similar behavior at all K values]. Figure 7 shows the variation of r_a as a function of K. As discussed in the Introduction, at very low values of the coupling the nodes are uncoupled, leading us to expect low values of r_a. In fact, we observe three distinct values of r_a, depending on initial condition, for the following reasons. In the case of a single peak initial condition, most of the nodes in the network are initially "synchronized" at zero (leading to an accordingly larger initial value of r_a), while in a random initial condition there can be some nodes that start with similar values; in the sine wave initial condition there is a smooth variation of amplitude instead of multiple repeated values.

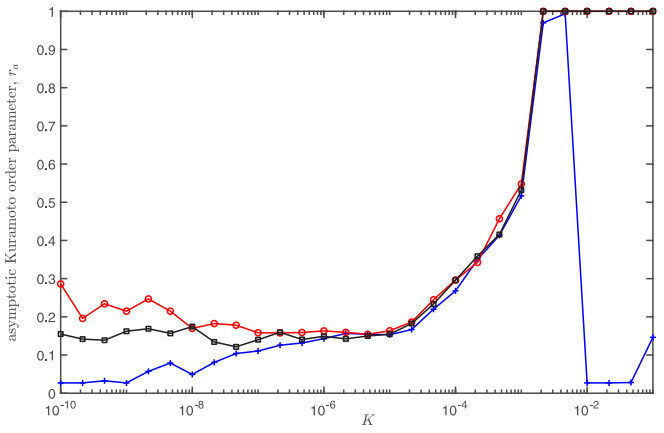

FIG. 7. Asymptotic value of the Kuramoto order parameter, $r_a = \lim_{t\to\infty} r(t)$, as a function of the coupling coefficient K for different initial conditions: the case of a single peak initial condition (red lines with circles), a sine wave initial condition (blue lines with crosses), and a uniformly distributed random initial condition (black line with square markers).

In contrast, at large values of K, all nodes in the network may be fully synchronized, leading us to expect $r_a \approx 1$. This is indeed the behavior that we observe for the single-peak and random initial conditions at large values of K. However, for the sine initial condition with the smoothest variation of amplitude (shown in blue line with plus markers), we observe that at large values of K, r_a falls sharply to very low values. We explain this as follows. Individual oscillators want to undergo regular periodic oscillations under the chosen parameter conditions. However, at large K, diffusion is strong enough to overcome such oscillations and causes the amplitude at every location in the ring to decay with time. In the asymptotic limit we then obtain small values for the Kuramoto order parameter r_a, indicative of effectively random phases computed from vanishingly small amplitudes. The final slight increase in $r_a \approx 0.15$ is a consequence of further increase in the coupling strength K.

Of course, the observed behavior for increasing values of the coupling coefficient K is also related to the initial amplitude distribution. In order to explore this dependence further, we show in Fig. 8 a similar plot of the asymptotic Kuramoto order parameter r_a as a function of K for the single peak and the sine wave initial condition starting with a larger initial amplitude distribution. The Riemann sums of the $\mathcal{A}_i(t = 0)$ for both initial conditions are again identical and the sine wave has a maximum value of 1×10^{-2}. We find that in both cases the evolution is able to reach fully synchronized behavior, $r_a \approx 1$, at large values of K. In this case, the sine wave initial

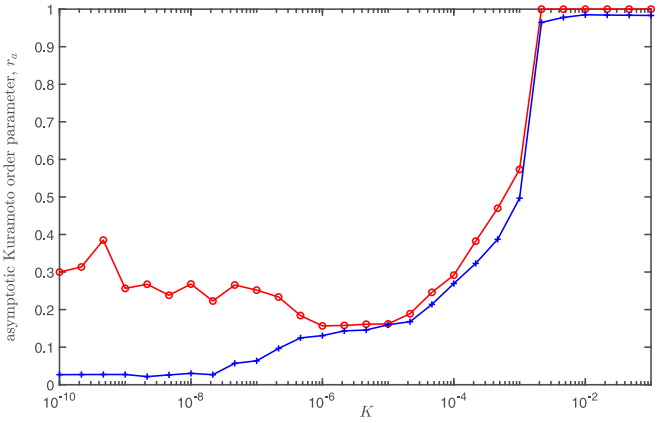

FIG. 8. Asymptotic value of the Kuramoto order parameter, $r_a = \lim_{t\to\infty} r(t)$, as a function of the coupling coefficient K for the single peak initial condition (red lines with dots) and the sine wave initial condition (blue lines with crosses) starting with a larger initial amplitude distribution.

condition is able to overcome diffusion at large K values to retain the regular periodic oscillations at every oscillator in the ring, resulting in large values of r_a.

D. Precursors for a high amplitude excursion

As observed from the probability density function results (Figs. 5 and 6) as well as the space-time plots (Fig. 2), the location $N_{\max}$ and the peak amplitude $\mathcal{A}_{\max}$ cannot be directly predicted during the evolution of the coupled oscillator network. However, there is great interest in being able to identify precursors that can indicate an impending large amplitude excursion in the form of a spatiotemporal rogue event. Previous work [38] combined statistical analysis along with a nonlinear stability criterion for a local wave train to quantify the probability of the occurrence of a large amplitude event. These authors also identified a simpler precursor which only tracks the energy of the wave field within an identified critical length scale. Both these measures rely on the assumption that the basin boundary for a rogue event is low dimensional. A separate approach, that considers such waves as hydrodynamic instantons that can be analyzed within the framework of large deviation theory and computed via suitably tailored numerical methods, is explored in [39]. Since the dynamics of the oscillator ring is by construction related to the dynamics of a single oscillator, we opt here to leverage the known low-dimensional dynamics of a single oscillator to design a qualitative diagnostic that can identify impending large and rapid growth of amplitude at a given location in the network.

In Fig. 9 we review the behavior during rogue events by plotting the amplitude $\mathcal{A}(t)$ of the $N_{\max} = 19$ oscillator in a semilogarithmic plot for the evolution shown in the right panel of Fig. 2. Each large amplitude excursion is noted in different colors: blue (between 1 and 2), black (between 2 and 3), and red (between 3 and 4). Superimposed on this evolution and shown as brown circles are instances when our precursor P (see the relevant definition below) indicates that

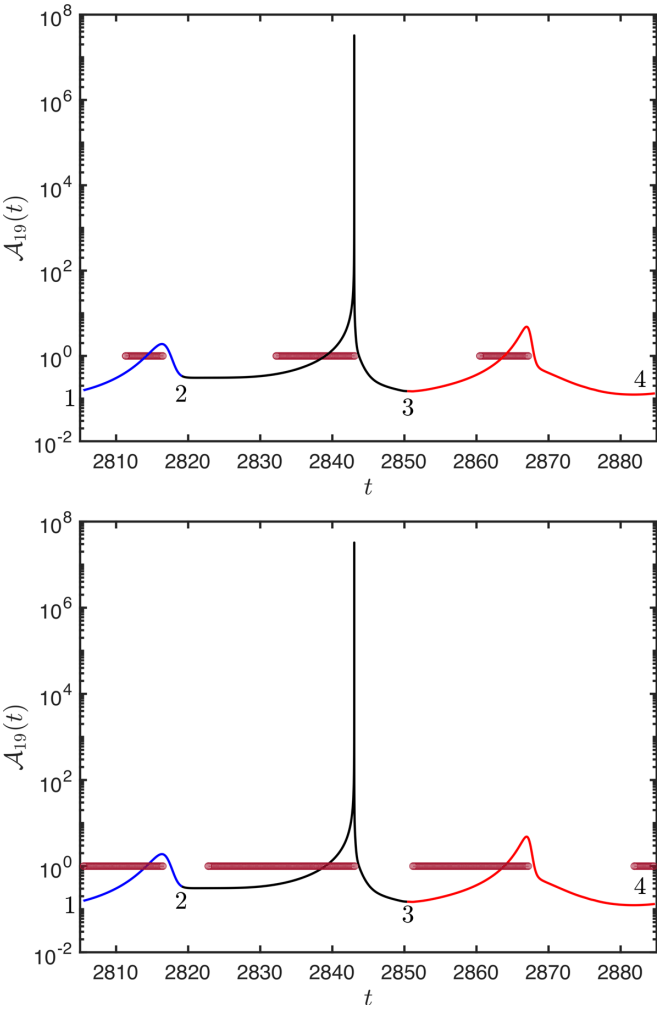

FIG. 9. Large amplitude events at $i = 19$ as seen in the right panel of Fig. 2 in the time domain shown superposed on locations where the precursor P identifies rapid growth (brown circles) due to the alignment of the trajectory with the stable direction of the saddle solution u_∞ (top panel) and of the v_∞ solution (bottom panel) of a single uncoupled oscillator.

the evolution is heading toward a large amplitude excursion. We observe that the qualitative precursor is able to identify each of the imminent large amplitude excursions well before the amplitudes have reached large values and independent of the amplitude at which the growth commences. In the rest of this section we detail how we construct this precursor.

The change of variables in Eq. (2) allows us to identify the large amplitude events as $\mathcal{A} = \rho^{-1}$, where $\rho \ll 1$. The limit of $\rho = 0$ corresponds to the invariant subspace Σ_∞, as this is the limit for which the amplitude $\mathcal{A} \to \infty$. In the following we denote the u and v solutions in Σ_∞ with the subscript ∞.

Figure 10 shows the trajectory (after an initial transient) of both the single uncoupled oscillator (in green, top panel) and the $i = 19$ oscillator on a ring with $K = 2.1544 \times 10^{-6}$ (in blue, black, and red colors, bottom panel) projected onto the variables ρ and ϕ. In this figure, red markers (pluses, circles, and triangles) in the panels indicate the locations of the invariant solutions for an uncoupled oscillator in the (ρ, θ, ϕ) variables. Circles indicate solutions of the so-called u_∞ type

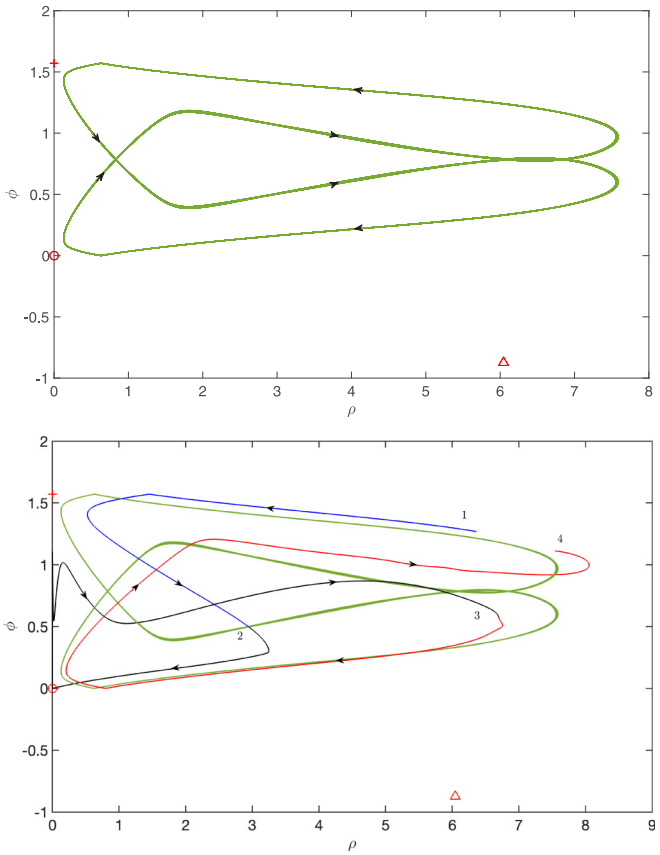

FIG. 10. Top: Phase portrait in the (ρ, ϕ) plane during regular periodic spiking at a single node in the network with no coupling (green line). Bottom: Same view in the (ρ, ϕ) plane with superposed evolution close to the large amplitude event at $i = 19$ (black line) in the coupled network with $K = 2.1544 \times 10^{-6}$, for comparison with Fig. 9.

[33,34], pluses indicate solutions of v_∞ type, and triangles indicate finite amplitude solutions that are mixed u/v states. These three solutions represent fixed points of the (ρ, θ, ϕ) system in Eqs. (A1) of the Appendix and represent traveling states of the underlying individual oscillator dynamics described by Eqs. (1) with the chosen level of asymmetry at the parameters given in Eq. (3).

For this oscillator, we calculate the eigenvalues of each solution in the Σ_∞ subspace [34] and find that the point u_∞ at $(\rho, \theta, \phi) = (0, \pi/2, 0)$ is a saddle (red circle in Fig. 10, top panel), while v_∞ at $(\rho, \theta, \phi) = (0, \pi/2, \pi/2)$ is an unstable spiral (red plus in Fig. 10, top panel). Integration of Eqs. (A1) reveals a stable periodic spiking orbit (green line in the top panel, black arrows indicating direction of forward time) that periodically approaches both u_∞ and v_∞, i.e., small values of ρ. Both of these excursions correspond to amplitude spikes, with no discernible difference between them. We expect the dynamics of a diffusively coupled ring of such nodes to follow this orbit at small values of diffusive coupling K. Indeed, when all the oscillators in the ring are initialized with this same periodic state and the same temporal phase, the coupled evolution on the ring retains this synchronization. This means that the rogue event-bearing state observed for the oscillator ring coexists with the synchronized periodic oscillation reflecting the dynamics of a single uncoupled oscillator.

In Fig. 10, bottom panel, we superimpose the evolution of the $i = 19$ node in the diffusively coupled ring shown previously in Fig. 9 on the dynamics of the uncoupled system (top panel, green trajectory), both projected on the (ρ, ϕ) plane. The blue, black, and red parts of the trajectory match those in Fig. 9. Between points 1 and 2 (segment shown in blue) the solution approaches v_∞ (red plus). This approach is responsible for the first spike in Fig. 9. Beyond point 2 (segment shown in black) the trajectory is able to return to extremely small values of ρ, $\rho = 4.39 \times 10^{-9}$, but this time due to an approach to u_∞ (red circle). This close approach is responsible for the very large amplitude spike in Fig. 9. Beyond point 3 (segment shown in red), the trajectory returns to u_∞ but does not reach such small values of ρ. This excursion is responsible for the third spike in Fig. 9. Thus the evolution of the $i = 19$ oscillator recapitulates the dynamics of a single oscillator, but does so irregularly and with occasional excursions close to the $\rho = 0$ fixed points, resulting in a large amplitude spike, i.e., a rogue wave. This comparison also suggests that the coupling to nearest neighbors may occasionally lead to smaller values of ρ (i.e., bigger spikes) as in the segment from 2 to 3, but also to larger values of ρ, as in the segment from 3 to 4.

Given that the uncoupled dynamics has a pair of saddles in the Σ_∞ subspace, we can expect a large amplitude excursion if the evolution is aligned with the stable direction of the saddle u_∞, say, which we will call $\bar{V}_1$. Further, we expect the amplitude to continue to grow until the projection of the current state on the fastest unstable eigendirection of the saddle u_∞, which we will call $\bar{V}_2$, starts to increase. We use the above notions to design a qualitative precursor for a large amplitude excursion as follows:

$$P = \begin{cases} 1 & \text{if } \mathcal{P}\,(state, \bar{V}_1) > 0 \text{ and } \mathcal{P}(state, \bar{V}_2) \\ & \text{is decreasing in time} \\ 0 & \text{otherwise.} \end{cases} \tag{7}$$

Here $\mathcal{P}$ is the projection of the current state along the respective eigendirection $\bar{V}_1$ or $\bar{V}_2$. With the above definition, we identify instances in time where the local dynamics is aligned close to the attracting direction of the saddle u_∞ and is not evolving along the unstable direction of u_∞. We determine the temporal variation of the projection of the current state along $\bar{V}_2$ via a simple first order approximation of the derivative. When both these conditions are satisfied and $P = 1$, we expect the dynamics to continue to evolve along the stable direction $\bar{V}_1$ of the saddle u_∞, implying that $\rho \to 0$ and the amplitude therefore grows. This condition is what we identify as a qualitative precursor of an impending large amplitude excursion. When these conditions are not satisfied, we have $P = 0$ and we do not expect to see a large amplitude event.

As already mentioned, overlaid on the amplitude evolution in Fig. 9, top panel, and shown in brown circles are time instances where the above criterion predicts a precursor event ($P = 1$), indicating that a large amplitude excursion is imminent. We see that this diagnostic is able to identify the growth intervals of all three amplitude excursions regardless of which fixed point in Σ_∞ is approached. A similar definition of a precursor can also be created with respect to the eigendirections of the v_∞ solution (Fig. 9, bottom panel). Thus, estimating to

what extent the current state of a node in a coupled ring of oscillators maps on the dynamics of a single uncoupled oscillator allows us to identify impending large amplitude events in this system. We believe that this type of diagnostic could be relevant to other systems, provided that a mathematical characterization of the large amplitude solutions of a single uncoupled node is available.

E. Amplitude-dependent diffusive coupling

Having examined the case of uniform coupling across the nodes of our ring, we now wish to explore the potential impact of heterogeneity in the lattice coupling (cf. [40–42]). Specifically, we suppose that the spatial coupling depends on the current value of $z_\pm$ via the amplitude $\mathcal{A}$ according to

$$K_i = K_0 \mathcal{A}_i(t) = K_0(|z_{i+}|^2 + |z_{i-}|^2), \tag{8}$$

with K_0 being a tunable parameter.

Here we observe some qualitative differences in the behavior of the system for different initial conditions. As shown in Fig. 11, for the single peak initial condition (red lines with circle markers) the maximal events observed are much larger, occur much earlier in the evolution (compared to other initial conditions), and are all concentrated at the location of the initial peak. This is expected, as the vast majority of the lattice nodes is initialized with near-vanishing amplitude thereby preventing the outward propagation of the initial disturbance even for $K_0 \neq 0$. In contrast, the random and sine distributed initial conditions are observed to yield excitations with lower amplitudes over the whole range of K_0 considered. For the sine wave initial condition, these mostly occur at the locations of the peaks in the sine wave initial condition while there is no preferential location for the random initial condition. As expected, the single peak initial condition can only exhibit rogue events at the location that is initialized with nonzero amplitude.

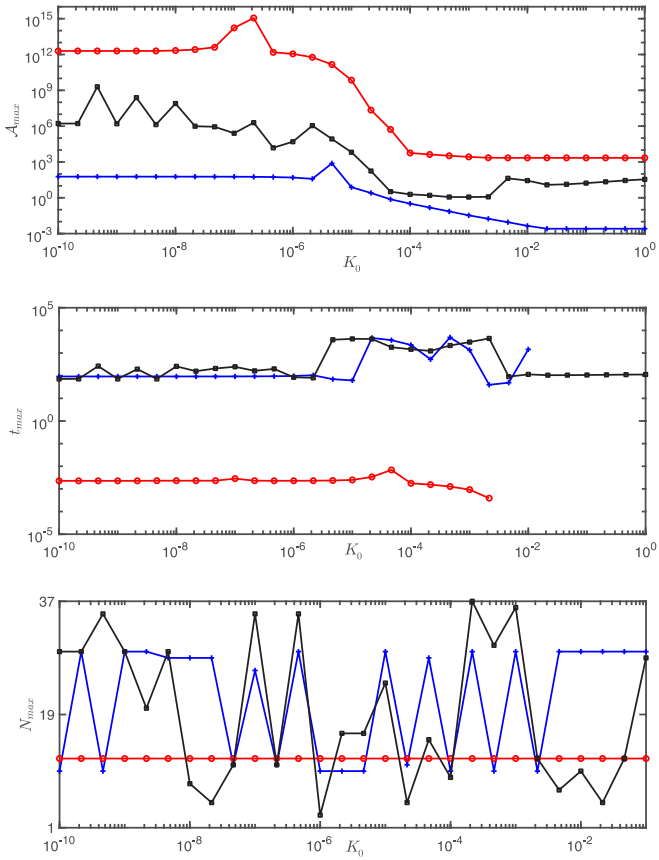

FIG. 11. Same as Fig. 6 but for the amplitude-dependent coupling (8). Red lines with circle markers show results for the single peak initial condition while blue lines with plus markers are the results for the sine wave initial condition. The top panel shows the variation in the maximum amplitude of observed excitations (on logarithmic scale) as a function of the coupling coefficient K_0. The middle panel shows the variation in the time taken to reach the maximal excitation $t_{\max}$ on logarithmic scale, also as a function of K_0. Finally, the bottom panel shows the variation of the location $N_{\max}$ of the maximal amplitude among the individual oscillators as a function of K_0. Note that the single peak initial conditions were initialized at $i = 12$.

III. CONCLUSIONS AND FUTURE CHALLENGES

In this work we have revisited a system that is known to exhibit bursting over a coherent region of space, and reformulated the problem to permit the activation of spatial degrees of freedom. We found that the resulting system could indeed generate extreme events that were localized in both time and space, and that occurred more or less at random locations on a periodic ring of such bursters and at random times. Our system offers an intriguing alternative to more conventional studies of rogue wave formation based on integrable Hamiltonian partial differential equations, typically the nonlinear Schrödinger equation and its variants. The latter approach has met with considerable success, and there is good evidence that rogue waves resembling the Peregrine soliton [25] and its periodic and higher order generalizations do in fact occur in wave experiments in a channel geometry (see, e.g., [10]). Our aim has been to propose an alternative mechanism that could give rise to such extreme events in distributed forced dissipative lattice systems. The proposed mechanism is fundamentally based on a strong resonance between two almost degenerate modes and has the remarkable property that it permits excitations of *arbitrarily* large amplitude. The model has the welcome additional property that its dynamics "at infinity" is well understood.

We considered a nonlinear dynamical lattice consisting of diffusively coupled elements of the above type, and demonstrated that such lattices can manifest a phenomenon resembling rogue events, i.e., waves that "appear out of nowhere and disappear without a trace" [32]. We showed in particular that such events may be present even when the individual oscillators oscillate periodically, and explained how this behavior depends on the (weak) diffusive coupling between the oscillating elements. In addition, we demonstrated the possibility of synchronization at larger coupling strength, quantified the distribution of the rogue amplitudes in terms of a bimodal probability distribution, and examined the synchronization properties of the system using Kuramoto-type order parameter diagnostics. Importantly, we also presented

an approach that enabled us to predict reliably impending rogue events through a quantitative understanding of (infinite amplitude) solutions and their eigenvector characteristics. We believe that this approach is suitable for implementing machine learning techniques for lattice systems, and will explore this approach in a future publication.

As already mentioned we may think of Eqs. (1) as the amplitude equations for nearly resonant oscillations in, for example, binary fluid convection in a moderately large domain of length L_0, say, where the variables $z_\pm$ represent the amplitudes of odd and even standing waves. An explicit derivation of the amplitude equations would necessarily lead to Eqs. (1) while also recovering the parameter dependence of the coefficients in these equations but remains to be done (see [43] for a related steady state problem). We expect that in larger domains, where the domain length L is inversely linked to the amplitude parameter ϵ via $L \sim L_0\epsilon^{-\alpha}$, $\alpha > 0$, one would in addition obtain spatial derivatives describing the large scale spatial modulation of these amplitudes as in Eqs. (4), much as in the standard derivation of the complex Ginzburg-Landau equation, albeit here for the case with two nearly degenerate carrier wave numbers. In such an equation, the coupling coefficient K would quantify the (squared) scale ratio $\epsilon^{2\alpha} \ll 1$ which is expected to be a small quantity in the original variables. Additional realizations of Eqs. (4) are readily envisaged.

Our emphasis on strong resonance between nearly degenerate modes differs fundamentally from alternative approaches based on the nonlinear evolution of modulational instabilities but connects the rogue wave phenomenon to the dynamics of systems exhibiting large amplitude sloshing [44,45], and our system is arguably one of the simplest ones of this type. We have leveraged the behavior of coupled oscillators with approximate 1:1 temporal resonance [46] but incorporated in our approach the possibility that standing oscillations are themselves unstable to traveling modes (cf. [47]). It is ultimately this destabilization of the standing mode that permits the large amplitude bursting behavior present in our model. This is, in fact, precisely the situation that arises in binary fluid convection with typical binary mixture parameters [48]. The spatial coupling of our bursting elements is designed to activate scales larger than the length scale L_0 of each element and hence captures the dynamics of large scale systems where similar destabilization is present [49]. Other one-dimensional lattices, consisting, for example, of Duffing oscillators with resonant forcing [50] or optical cavity arrays [51], may also exhibit localized structures in space-time, but without the dynamic range admitted by the system studied in the present work.

Naturally, there exist numerous directions for further study. While we have given here a proof of principle of localized dynamics in space-time, it does not escape us that the original ODE system in Eqs. (1) possesses a substantial wealth of additional possible states as the relevant parameters vary [33,34]. In this light, a further study of the role of such additional states, especially those in the invariant subspace at infinite amplitude, in the dynamics of our diffusively coupled lattice system is certainly merited, as is a study of the effect of random coupling strengths between adjacent nodes, be these quenched or stochastically varying in time [40–42]. Moreover, the mechanism of extreme event production put forth herein is not restricted to one-dimensional lattices (as is often the case for integrable Hamiltonian systems) but generalizes naturally to higher dimensions, a topic also worth exploring in its own right. Such studies are currently in progress and will also be reported in a future publication.

ACKNOWLEDGMENTS

P.G.K. gratefully acknowledges discussions with Ji Hun (Jimmy) Hwang whose honors thesis provided some early-stage dynamical simulations for the lattice system considered herein. This material is based upon work supported by the U.S. National Science Foundation under Grants No. DMS-1908891 (E.K.) No. PHY-2110030 (P.G.K.), as well as No. DMS-2204702 (P.G.K.). E.K. and P.G.K. also gratefully acknowledge Professor I. G. Kevrekidis for initiating their discussions on this topic.

APPENDIX: THE (ρ, θ, ϕ) SYSTEM

We consider the (ρ, θ, ϕ) formulation from [34] in terms of a rescaled time $d\tau/dt = 1/\rho$. In this formulation Eqs. (1) become

$$\begin{aligned}
\frac{d\rho}{d\tau} &= \rho(2A_R + B_R(1+\cos^2\theta) + C_R\sin^2\theta\cos 2\phi) \\
&\quad - 2(\lambda + \triangle\lambda\cos\theta)\rho^2, \\
\frac{d\theta}{d\tau} &= \sin\theta(\cos\theta(-B_R + C_R\cos 2\phi) - C_I\sin 2\phi) \\
&\quad - 2\triangle\lambda\rho\sin\theta, \\
\frac{d\phi}{d\tau} &= \cos\theta(B_I - C_I\cos 2\phi) - C_R\sin 2\phi + 2\triangle\omega\rho, \qquad \text{(A1)}
\end{aligned}$$

where the subscripts R and I indicate real and imaginary parts. In order to determine equilibria for this set of equations, we recast these equations in terms of the state vector

$$X = (X_1, X_2, X_3, X_4, X_5) = (\rho, \cos\theta, \sin\theta, \cos 2\phi, \sin 2\phi).$$

With this new state vector, the governing dynamics constitutes a system with constant coefficients, which implies that its equilibria can be determined by solving the associated set of polynomial equations,

$$\begin{aligned}
-X_1\left[2A_R + B_R\left(1 + X_2^2\right) + C_R X_3^2 X_4\right] - 2(\lambda + \triangle\lambda X_2)X_1^2 &= 0, \\
X_3[X_2(-B_R + C_R X_4) - C_I X_5] - 2\triangle\lambda X_1 X_3 &= 0, \\
X_2(B_I - C_I X_4) - C_R X_5 + 2\triangle\omega X_1 &= 0, \\
X_2^2 + X_3^2 - 1 &= 0, \\
X_4^2 + X_5^2 - 1 &= 0. \qquad \text{(A2)}
\end{aligned}$$

Here the last two equations arise from the conditions that must be satisfied by the transformation of the sine and cosine functions into the new variables. In this recast form, we have a fully determined system of polynomial equations for the five unknowns and we use homotopy methods to determine all real, finite, and nontrivial solutions of the resulting system using BERTINI [52].

[1] C. Kharif and E. Pelinovsky, Physical mechanisms of the rogue wave phenomenon, Eur. J. Mech. B Fluids **22**, 603 (2003).

[2] M. Onorato, S. Residori, U. Bortolozzo, A. Montina, and F. T. Arecchi, Rogue waves and their generating mechanisms in different physical contexts, Phys. Rep. **528**, 47 (2013).

[3] E. Pelinovsky and C. Kharif, *Extreme Ocean Waves* (Springer, Cham, 2016), pp. 1–236.

[4] A. R. Osborne, *Nonlinear Ocean Waves and the Inverse Scattering Transform* (Elsevier, Amsterdam, 2010).

[5] N. Mori and P. C. Liu, Analysis of freak wave measurements in the Sea of Japan, Ocean Eng. **29**, 1399 (2002).

[6] S. Haver, A possible freak wave event measured at the Draupner jacket January 1 1995, Rogue Waves 2004: Proceedings of a Workshop, Brest, France (unpublished).

[7] D. A. G. Walker, P. H. Taylor, and R. E. Taylor, The shape of large surface waves on the open sea and the Draupner New Year wave, Appl. Ocean Res. **26**, 73 (2004).

[8] T. A. A. Adcock, P. H. Taylor, S. Yan, Q. W. Ma, and P. A. E. M. Janssen, Did the Draupner wave occur in a crossing sea? Proc. R. Soc. A **467**, 3004 (2011).

[9] A. Chabchoub, N. P. Hoffmann, and N. Akhmediev, Rogue Wave Observation in a Water Wave Tank, Phys. Rev. Lett. **106**, 204502 (2011).

[10] A. Chabchoub, N. Hoffmann, M. Onorato, and N. Akhmediev, Super Rogue Waves: Observation of a Higher-Order Breather in Water Waves, Phys. Rev. X **2**, 011015 (2012).

[11] M. L. McAllister, S. Draycott, T. A. A. Adcock, P. H. Taylor, and T. S. Van Den Bremer, Laboratory recreation of the Draupner wave and the role of breaking in crossing seas, J. Fluid Mech. **860**, 767 (2019).

[12] G. Xu, A. Chabchoub, D. E. Pelinovsky, and B. Kibler, Observation of modulation instability and rogue breathers on stationary periodic waves, Phys. Rev. Research **2**, 033528 (2020).

[13] D. R. Solli, C. Ropers, P. Koonath, and B. Jalali, Optical rogue waves, Nature (London) **450**, 1054 (2007).

[14] J. M. Dudley, F. Dias, M. Erkintalo, and G. Genty, Instabilities, breathers and rogue waves in optics, Nat. Photonics **8**, 755 (2014).

[15] B. Frisquet, B. Kibler, P. Morin, F. Baronio, M. Conforti, G. Millot, and S. Wabnitz, Optical dark rogue wave, Sci. Rep. **6**, 20785 (2016).

[16] A. Tikan, C. Billet, G. El, A. Tovbis, M. Bertola, T. Sylvestre, F. Gustave, S. Randoux, G. Genty, P. Suret, and J. M. Dudley, Universality of the Peregrine Soliton in the Focusing Dynamics of the Cubic Nonlinear Schrödinger Equation, Phys. Rev. Lett. **119**, 033901 (2017).

[17] E. G. Charalampidis, J. Cuevas-Maraver, D. J. Frantzeskakis, and P. G. Kevrekidis, Rogue waves in ultracold bosonic seas, Romanian Rep. Phys. **70**, 504 (2018).

[18] M. S. Ruderman, Freak waves in laboratory and space plasmas, Eur. Phys. J.: Spec. Top. **185**, 57 (2010).

[19] R. Sabry, W. M. Moslem, and P. K. Shukla, Freak waves in white dwarfs and magnetars, Phys. Plasmas **19**, 122903 (2012).

[20] A. S. Bains, B. Li, and L. D. Xia, Kinetic Alfvén solitary and rogue waves in superthermal plasmas, Phys. Plasmas **21**, 032123 (2014).

[21] R. E. Tolba, W. M. Moslem, N. A. El-Bedwehy, and S. K. El-Labany, Evolution of rogue waves in dusty plasmas, Phys. Plasmas **22**, 043707 (2015).

[22] R. Höhmann, U. Kuhl, H. J. Stöckmann, L. Kaplan, and E. J. Heller, Freak Waves in the Linear Regime: A Microwave Study, Phys. Rev. Lett. **104**, 093901 (2010).

[23] C. Sulem and P. L. Sulem, *The Nonlinear Schrödinger Equation: Self-Focusing and Wave Collapse* (Springer-Verlag, New York, 1999).

[24] M. J. Ablowitz, B. Prinari, and A. D. Trubatch, *Discrete and Continuous Nonlinear Schrödinger Systems* (Cambridge University Press, Cambridge, U.K., 2003).

[25] D. H. Peregrine, Water waves, nonlinear Schrödinger equations and their solutions, J. Aust. Math. Soc. Ser. B, Appl. Math. **25**, 16 (1983).

[26] E. A. Kuznetsov, Solitons in a parametrically unstable plasma, Sov. Phys. Dokl. **236**, 575 (1977).

[27] Y.-C. Ma, The perturbed plane-wave solutions of the cubic Schrödinger equation, Stud. Appl. Math. **60**, 43 (1979).

[28] N. N. Akhmediev and V. I. Korneev, Modulation instability and periodic solutions of the nonlinear Schrödinger equation, Theor. Math. Phys. **69**, 1089 (1986).

[29] A. Ankiewicz, N. Akhmediev, and J. M. Soto-Crespo, Discrete rogue waves of the Ablowitz-Ladik and Hirota equations, Phys. Rev. E **82**, 026602 (2010).

[30] C. Hoffmann, E. G. Charalampidis, D. J. Frantzeskakis, and P. G. Kevrekidis, Peregrine solitons and gradient catastrophes in discrete nonlinear Schrödinger systems, Phys. Lett. A **382**, 3064 (2018).

[31] S. Coulibaly, M. Taki, A. Bendahmane, G. Millot, B. Kibler, and M. G. Clerc, Turbulence-Induced Rogue Waves in Kerr Resonators, Phys. Rev. X **9**, 011054 (2019).

[32] N. Akhmediev, A. Ankiewicz, and M. Taki, Waves that appear from nowhere and disappear without a trace, Phys. Lett. A **373**, 675 (2009).

[33] J. Moehlis and E. Knobloch, Forced Symmetry Breaking as a Mechanism for Bursting, Phys. Rev. Lett. **80**, 5329 (1998).

[34] J. Moehlis and E. Knobloch, Bursts in oscillatory systems with broken D_4 symmetry, Physica D **135**, 263 (2000).

[35] E. Knobloch and J. Moehlis, Bursts, in *Proceedings IUTAM Symposium on New Applications of Nonlinear and Chaotic Dynamics in Mechanics*, edited by F. C. Moon (Kluwer Academic, Dordrecht, 1998), pp. 51–60.

[36] T. S. Sullivan and G. Ahlers, Nonperiodic time dependence at the onset of convection in a binary liquid mixture, Phys. Rev. A **38**, 3143 (1988).

[37] S. H. Strogatz, From Kuramoto to Crawford: Exploring the onset of synchronization in populations of coupled oscillators, Physica D **143**, 1 (2000).

[38] W. Cousins and T. P. Sapsis, Reduced-order precursors of rare events in unidirectional nonlinear water waves, J. Fluid Mech. **790**, 368 (2016).

[39] G. Dematteis, T. Grafke, M. Onorato, and E. Vanden-Eijnden, Experimental Evidence of Hydrodynamic Instantons: The Universal Route to Rogue Waves, Phys. Rev. X **9**, 041057 (2019).

[40] Y. Braiman, W. L. Ditto, K. Wiesenfeld, and M. L. Spano, Disorder-enhanced synchronization, Phys. Lett. A **206**, 54 (1995).

[41] Y. Sugitani, Y. Zhang, and A. E. Motter, Synchronizing Chaos with Imperfections, Phys. Rev. Lett. **126**, 164101 (2021).

[42] Y. Zhang, J. L. Ocampo-Espindola, I. Z. Kiss, and A. E. Motter, Random heterogeneity outperforms design in network synchronization, Proc. Natl. Acad. Sci. U.S.A. **118**, e2024299118 (2021).

[43] P. Hirschberg and E. Knobloch, Mode interactions in large aspect ratio convection, J. Nonlinear Sci. **7**, 537 (1997).

[44] B. W. Zeff, B. Kleber, J. Fineberg, and D. P. Lathrop, Singularity dynamics in curvature collapse and jet eruption on a fluid surface, Nature (London) **403**, 401 (2000).

[45] O. M. Faltinsen and A. N. Timokha, *Sloshing* (Cambridge University Press, New York, 2009).

[46] P. H. Steen and S. H. Davis, Quasiperiodic bifurcation in nonlinearly-coupled oscillators near a point of strong resonance, SIAM J. Appl. Math. **42**, 1345 (1982).

[47] J. D. Crawford and E. Knobloch, Symmetry and symmetry-breaking bifurcations in fluid mechanics, Annu. Rev. Fluid Mech. **23**, 341 (1991).

[48] W. Schöpf and W. Zimmermann, Multicritical behaviour in binary fluid convection, Europhys. Lett. **8**, 41 (1989).

[49] O. Batiste, E. Knobloch, I. Mercader, and M. Net, Simulations of oscillatory binary fluid convection in large aspect ratio containers, Phys. Rev. E **65**, 016303 (2001).

[50] F. Fontanela, A. Grolet, L. Salles, A. Chabchoub, A. R. Champneys, S. Patsias, and N. Hoffmann, Dissipative solitons in forced cyclic and symmetric structures, Mech. Syst. Signal Process. **117**, 280 (2019).

[51] A. V. Yulin and A. R. Champneys, Discrete snaking: Multiple cavity solitons in saturable media, SIAM J. Appl. Dyn. Syst. **9**, 391 (2010).

[52] D. J. Bates, J. D. Haunstein, A. J. Sommese, and C. W. Wampler, *Numerically Solving Polynomial Systems with Bertini* (Society for Industrial and Applied Mathematics, Philadelphia, 2013).